International Journal of Biological Macromolecules 101 (2017) 51–58

Contents lists available at ScienceDirect

International Journal of Biological Macromolecules

journal homepage: www.elsevier.com/locate/ijbiomac

Development of nanocomposite scaffolds based on TiO_2 doped in grafted chitosan/hydroxyapatite by freeze drying method and evaluation of biocompatibility

Saber Abd-Khorsand [a], Samaneh Saber-Samandari [b,*], Saeed Saber-Samandari [c,*]

[a] Materials and Biomaterials Research Center, Tehran, Iran
[b] Department of Chemistry, Eastern Mediterranean University, Gazimagusa, TRNC via Mersin 10, Turkey
[c] New Technologies Research Center, Amirkabir University of Technology, Tehran, Iran

ARTICLE INFO

Article history:
Received 14 January 2017
Received in revised form 2 March 2017
Accepted 13 March 2017
Available online 16 March 2017

Keywords:
Bone tissue engineering
Scaffold
Titanium dioxide
Hydroxyapatite
Chitosan

ABSTRACT

Porous three-dimensional scaffolds with potential for application as cancellous bone graft substitutes were prepared using the freeze-drying technique. Hydroxyapatite with different weight ratio was embedded in the network of poly(acrylic acid) grafted chitosan accompanied by using TiO_2 as an auxiliary component to fabricate porous nanocomposite bone scaffolds. Fourier transform infrared spectroscopy, scanning electron microscopy, energy-dispersive X-ray spectroscopy, and X-ray diffraction analysis and mechanical tests were carried out to characterize the prepared scaffolds. These scaffolds showed well-controlled and interconnected porous structures. The pore size and porosity of the scaffolds could be effectively modulated by selecting appropriate amounts of hydroxyapatite. The results obtained from mechanical properties measurements indicated that the scaffolds could basically retain their strength in their dry state and have adequate mechanical properties close to those of cancellous bone. The swelling behavior of the scaffolds was also examined in both water and phosphate buffer saline solution. The cytotoxicity of the scaffold was determined by MTT assays on human fibroblast gum (HuGu) cells for 24, 48 and 72 h. In conclusion, this investigation demonstrates that the fabricated nanocomposite scaffolds are suitable for bone tissue engineering.

1. Introduction

Millions of people encounter bone defects because of trauma, tumor, natural ageing, bone fractures, obesity and indigent physical activity around the world [1]. In order to treat these defects, autografts, allografts and xenografts have been implemented but all have problems such as donor shortage, immune system response and disease transmission. Therefore, researchers in bone tissue engineering have approached a way to create a three-dimensional porous structure that mimics the bone and has overcome the mentioned problems using new natural and synthetic materials in forms of scaffolds. This porous scaffold should possess the properties of a natural bone such us biocompatibility, osteoconductivity, high porosity and reasonable mechanical strength [2,3].

The bone consists of ample amount of proteins and minerals. It possesses a two phase organic and inorganic structure which is made up of type I collagen, glycosaminoglycans, proteoglycans, glycoprotein and calcium phosphate [4]. The most dominant (60–65%) ceramic phase in bone is hydroxyapatite (HAp) with chemical formula of $Ca_{10}(PO_4)_6(OH)_2$. HAp as a bone substitute has drawn much attention because of its osteoconductive, bioactive, biocompatible properties [5]. It also bears excellent chemical and biological affinity with bony tissue [6]. Despite its many biological merits, HAp is brittle but the use of polymers and creating a ceramic/polymer composite scaffold can overcome this issue [7–10]. Many HAp/polymeric scaffolds have been studied over the past years and HAp/chitosan composite is highly appealing among them [11,12]. Chitosan (CS) is a linear copolymer of β-(1 → 4) linked 2-acetamido-2-deoxy-β-D-glucopyranose and 2- amino-2-deoxy-β-D-glycopyranose. It is retrieved by deacetylation of its parent polymer chitin, a polysaccharide widely distributed in nature (e.g. crustaceans, insects and certain fungi) [13]. CS is a non-toxic, biodegradable, anti-bacterial and hemostatic active natural polymer. Due to its hydrophilic surface it can promote cell adhesion,

* Corresponding authors.
E-mail addresses: samaneh.saber@gmail.com (S. Saber-Samandari), saeedss@aut.ac.ir (S. Saber-Samandari).

http://dx.doi.org/10.1016/j.ijbiomac.2017.03.067
0141-8130/

proliferation and differentiation [14,15]. In spite of versatile characteristics, unmodified CS also shows poor wet-state mechanical properties [16] and fast degradation [17]. The major obstacle with CS/HAp composite scaffold is still lack of mechanical strength to carry load after insertion into the adult body. TiO_2 was chosen as an auxiliary material in the present investigation, since TiO_2 ceramic scaffolds as a bone substitute material attracted particular attention due to its excellent mechanical properties compared to other ceramic materials [18–20]. Titanium (Ti) is well established as a biomaterial for bone substitute [21] and has been used in a variety of clinical applications because it is corrosion resistant, light weight, and its surface is covered by a layer of TiO_2 believed to contribute to its overall biocompatibility [22,23]. In a very recent research, Kim et al. created an osteoinductive hybrid scaffold by using silk fibroin, TiO_2 and HAp. The results affirmed that the porous silk fibroin/TiO_2/HAp hybrid scaffold had improved osteoinductivity compared with the porous silk fibroin scaffold [24].

The aim of the present investigation was to develop novel scaffolds, based on TiO_2 doped in the network of poly (acrylic acid) grafted CS comprising various amount of n-HAp. In order to investigate the effect of ceramic composition in the physical, chemical and biological properties, four different nanocomposite scaffolds with different portions of CS/n-HAp were synthesized by freeze-drying technique. The morphology and structural characteristics were observed by scanning electron microscopy (SEM), Fourier transform infrared spectroscopy (FTIR), energy-dispersive X-ray spectroscopy (EDS), and X-ray diffraction analysis (XRD). The suitability of these scaffolds as bone substitute was analyzed. The mechanical properties of the scaffolds were measured by compressive test instrument. Furthermore, the swelling behavior of the scaffolds was also examined in both water and phosphate buffer saline (PBS) solution. Finally, cytotoxicity of the scaffolds was tested by culturing HuGu cells in vitro.

2. Experimental procedures

2.1. Materials

Medium molecular weight CS (Aldrich) with 75–85% deacetylation and potassium persulfate (BDH) as an initiator was used to synthesize the nanocomposite scaffold. Acetic acid 37% was used as solvent for CS. Acrylic acid (AAc) from Merck was used as a monomer and N,N'-methylene-bis-acrylamide from Aldrich was used as a crosslinker. Both were applied without further purification. Nano HAp powder (<100 nm particle size, ≥97%) and TiO_2 (<100 nm particle size, >99.7%) were supplied by Aldrich. In order to prepare PBS solution, sodium chloride, potassium chloride, sodium hydrogen phosphate, di-potassium hydrogen phosphate and hydrochloric acid, all from Merck, were used as received.

2.2. Synthesis of nanocomposite scaffolds

In a two-step procedure the nanocomposite scaffolds were prepared. (I) preparation of the nanocomposite powder, (II) dissolving of the prepared nanocomposite powder in a suitable solvent, freeze-drying and then preparation of TiO_2 doped in chitosan-graft-poly(AAc)/n-HAp scaffolds.

1.6% w/v CS was dissolved in 2% v/v diluted acetic acid solution. The prepared solution was transferred in a two-necked round-bottom flask fitted with a nitrogen gas inlet in a water bath at 60 °C and stirred continuously. As an initiator 0.04 g potassium persulfate was added to the CS solution. After 15 min, 0.25 mL AAc and *N,N'*-methylene-bis-acrylamide (0.04% of AAc) were added to the initiated CS solution as monomer and crosslinker, respectively. After 30 min, TiO_2 (0.2 g) with different known amounts of n-HAp powder (from 0.4 to 1.6 g) were added slowly, and the solution was stirred for 3 h. Grafting Poly(AAc) into CS was done by free radical polymerization method. In addition, TiO_2 and n-HAp were trapped in the network of CS-graft-poly(AAc). In the final stage, with removing the nitrogen gas flow and cooling the solution, the graft polymerization and crosslinking was stopped. In order to remove any unreacted monomer or homopolymer the suspension was vacuum-filtered, washed with a large amount of distilled water and was dried overnight in an oven at 50 °C. Different nanocomposite powders, containing 1:0.25, 1:0.5, 1:0.75 and 1:1 CS/n-HAp ratio containing constant amounts of poly(AAc) and TiO_2 were synthesized and the designations of the systems are summarized in Table 1.

In the second step, the prepared nanocomposite powder (0.4 g) was dispersed sufficiently in acetic acid/water mixture (1:10) with a powder/solution ratio of 1:10 to create a uniform paste. The paste was inserted into a cylindrical plastic mold ($2 \times 8\ cm^2$). In order to solidify and prompt solid-liquid phase separation, the molds were frozen at −80 °C for 24 h. Afterwards, the solidified mixture was located in a freeze dryer machine (FD-10, Pishtaz Engineering Co., Iran) for 2 days. Lastly, cylindrical nanocomposite scaffolds without any major deformation or shrinkage were obtained.

2.3. Characterization methods

The morphology of the prepared nanocomposite scaffolds was analyzed by SEM (JEOL, 6400). Samples were sputter coated with gold at an accelerating voltage of 15 kV. To measure the pore size, ImageJ software was used [25,26]. First, ten different cross-sectional SEM micrographs representing different regions of the scaffold were selected. Then, the dimensions of more than 30 pores were measured and averaged to obtain a mean pore size. The chemical structure of chitosan powder and the prepared nanocomposite powder was evaluated using a FTIR spectroscopy (Thermo Nicolet FTIR, Nexus 670) over the range of 400–4000 cm^{-1}. In order to investigate the crystallinity and phase content of the scaffolds, XRD method (Rigaku, Tokyo) has been applied. EDS was used for finding a chemical composition of the prepared scaffolds. Mechanical properties were investigated using a standard testing machine (SANTAM, STM-20, Iran) with a loading rate of 0.5 mm/min and the load cell was 20 kn. Load and displacement data were used to generate engineering stress–strain curves and to determine the compressive strength. Elastic modulus refers to the stiffness of an elastic material and is typically calculated by determining the slope of a stress-strain curve during the elastic region of a compressive strength test. Elastic modulus values for all samples were derived using the test results for compressive strength.

2.4. Determination of the prepared scaffold porosity

To define a porosity (%) of the prepared nanocomposite scaffolds, liquid displacement method was applied [27]. A fixed amount of water (V_1) was poured into a scaled cylinder. The cylinder was used for soaking the dried scaffold. Now the new volume of the cylinder containing water and the dried scaffold is V_2. Considering better water penetration, the scaffold was kept under water for 3 h until no air bubbles were observed. V_3 is the measured residual volume of water after removing the wet scaffold from the cylinder. The porosity (%) of the synthesized composite scaffolds was calculated by the following equation:

$$\text{porosity}\,(\%) = \frac{V_1 - V_3}{V_2 - V_3} \times 100 \qquad (1)$$

Table 1
Chemical composition of the prepared nanocomposite scaffolds and their average pore size and porosity.

Scaffolds identity	CS (g)	AAc (mL)	TiO_2 (g)	n-HAp (g)	Pore size (μm)	Porosity (%)
S1	1.6	0.25	0.2	0.4	207 ± 2	55 ± 1
S2	1.6	0.25	0.2	0.8	185 ± 1	63 ± 2
S3	1.6	0.25	0.2	1.2	153 ± 2	78 ± 1
S4	1.6	0.25	0.2	1.6	92 ± 2	81 ± 1

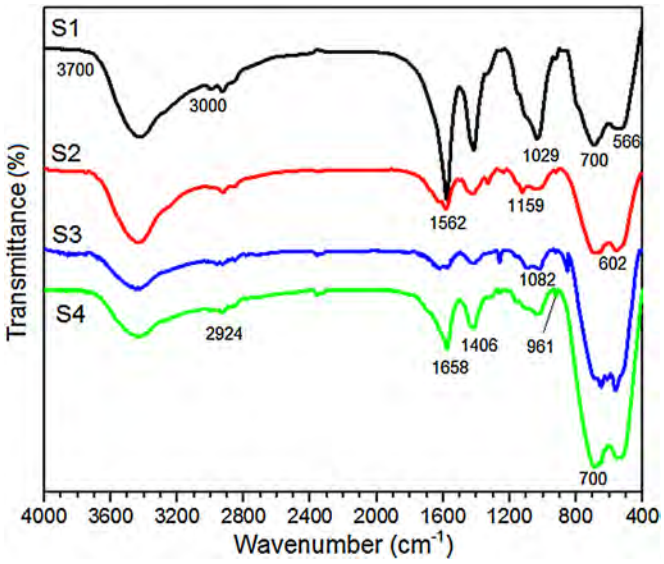

Fig. 1. The important peaks in FTIR spectra of the prepared nanocomposite scaffolds with different CS/n-HAp ratio of 1:0.25, 1:0.5, 1:0.75 and 1:1 (called S1, S2, S3 and S4) in the range of 400–4000 cm^{-1} were shown.

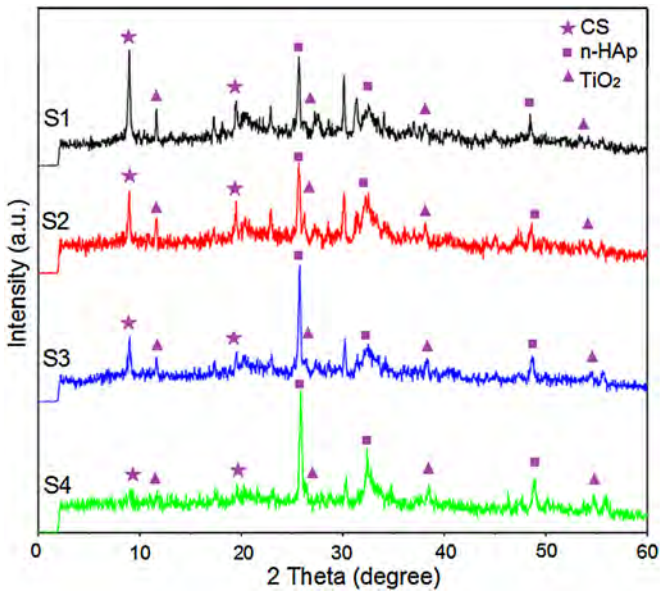

Fig. 2. The XRD patterns of the prepared nanocomposite scaffolds (S1-S4) was shown. The increase in intensity of apparent signals correspond to the n-HAp from S1 to S4 in the diagram confirm the presence of different amounts of n-HAp in the structure of the prepared nanocomposite scaffolds.

2.5. Swelling properties of the prepared scaffolds

The swelling property was characterized by immersing dried pieces of the prepared nanocomposite scaffolds (W_d) both in distilled water and PBS solution (with pH 7.4, at 37 °C). The PBS solution was prepared in the laboratory. To do so, 8 g NaCl, 0.2 g KCl, 1.44 g Na_2HPO_4, 0.25 g KH_2PO_4 were added to 800 mL of bi-distilled water. The solution was stirred for 5 min and then the pH was adjusted to 7.4 using a solution of hydrochloric acid (0.1 mol L^{-1}) in a dropwise manner. Finally, the total volume of PBS solution reached 1 L by the addition of extra bi-distilled water.

The scaffolds began to soak and imprison liquids in their pores for a time period until equilibrium was reached. The swollen nanocomposite scaffolds were taken out and weighed (W_s) after removing excess water on their surface. Lastly, the swelling (%) of the prepared nanocomposite scaffolds was calculated as follows:

$$\text{Swelling}\ (\%) = \frac{W_s - W_d}{W_d} \times 100 \quad (2)$$

2.6. Cell culture and MTT-base cytotoxicity assay

The 3-(4,5-dimethylthiazol-2-yl)-2,5-diphenyltetrazolium-bromide (MTT, Aldrich) assay, which was based on the extraction method, was applied to evaluate the cytotoxicity of the prepared nanocomposite scaffolds. First, Human gum fibroblast cells (HuGu) taken from the gums of a 45-year old female purchased from the Iranian Biological Resources Center (IBRC) was cultured in a fresh growth medium containing 89% high-glucose Dulbecco's Modified Eagle's Medium (DMEM), 2 mmol L^{-1} L-glutamine (Biochrom), 10% fetal bovine serum (FBS), and 1% penicillin (Merck). The cells were incubated at 37 °C in a humid atmosphere of 5% CO_2 and fed every 3 days. Second, the HuGu cells suspension with a concentration of 5000 cells in 100 μL of medium were placed into a 96-well culture plate in triplicate and incubated at 37 °C in an incubator. The plate was left undisturbed to allow cell attachment to occur. After seeding of the fibroblast cells, they were treated with five different concentrations of scaffold extracts (0.125–2.00 mg mL^{-1}) and was incubated. After 24, 48 and 72 h, the medium was aspirated and then 20 μL of MTT solution (5 mg mL^{-1} of PBS) was added to each well, including controls (cells seeded without the addition of the scaffolds extract). The last incubation was conducted for another 4 h at 37 °C. The upper solvent of wells was removed and formazan precipitate was solubilized with 200 μL of dimethyl sulfoxide (DMSO). Finally, the optical density values were recorded at 570 nm by the absorbance microplate reader (Bio-Tek, ELx-800, USA). The cell viability (%) is calculated as follows:

$$\text{Cell viability}\ (\%) = \frac{\text{OD}_{\text{Sample}}}{\text{OD Control}} * 100 \quad (3)$$

3. Results and discussion

3.1. Characterizations of the prepared scaffolds

3.1.1. Fourier transform infrared (FTIR) spectroscopy

Fig. 1 shows the FTIR spectrum of TiO_2 doped in CS-graft-poly(AAc)/n-HAp nanocomposite scaffolds with different n-HAp contents. As can be seen, the absorption bands observed at 1029, 1092, 961, 602 and 566 cm^{-1} correspond to symmetric and asymmetric stretching and bending vibrations of the PO_4^{3-} groups in n-HAp, which were improved by increasing the n-HAp contents in the nanocomposite scaffolds (from S1 to S4) [9,28]. It is noteworthy that the peaks below 700 cm^{-1} attributed to Ti—O and Ti—O—Ti

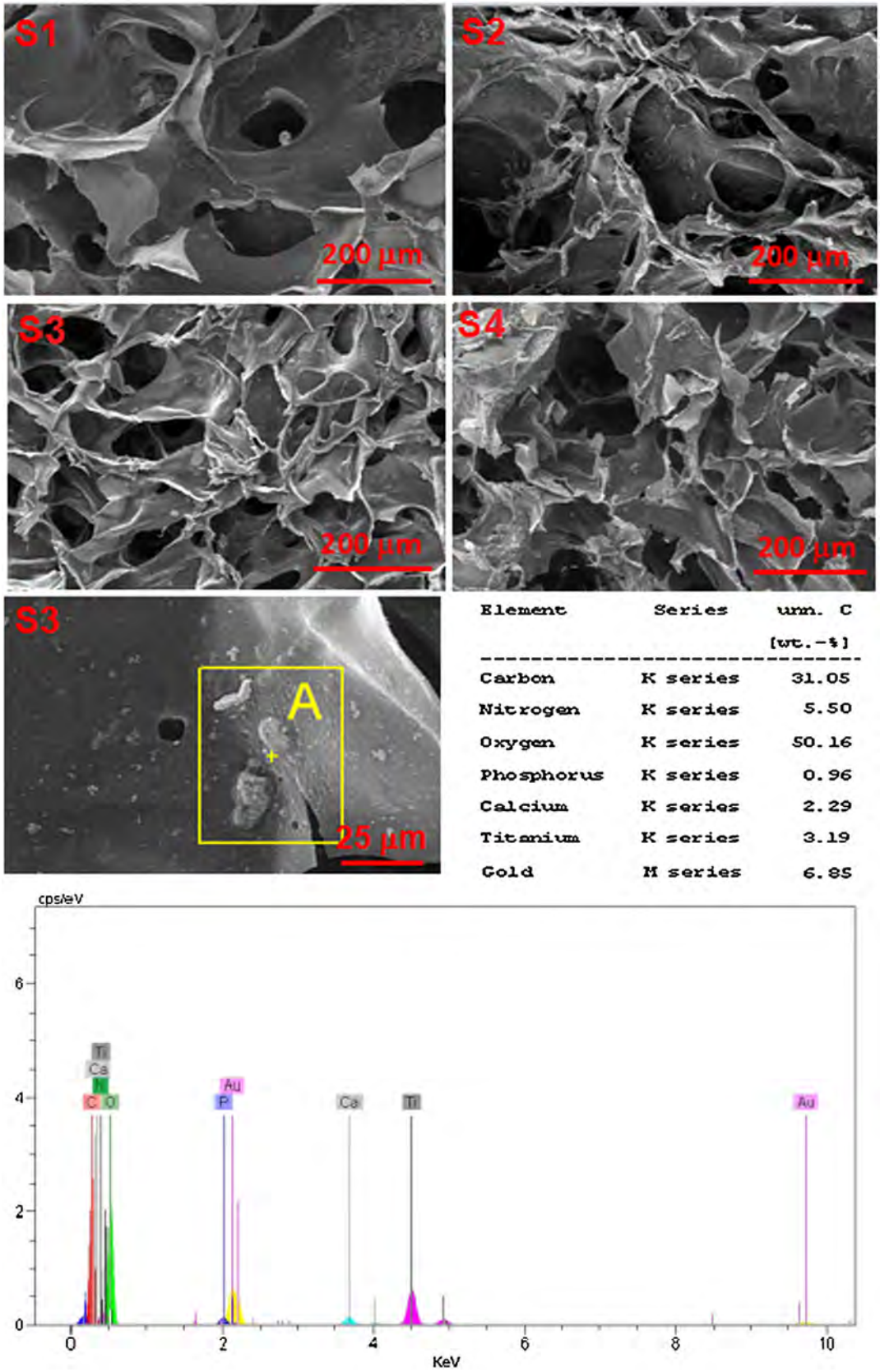

Fig. 3. The morphology of the prepared gold coated nanocomposite scaffolds (S1-S4) at an accelerating voltage of 15 kV, which was analyzed by SEM was shown. Also, elemental composition of the prepared nanocomposite scaffold (S3) was analyzed by EDS.

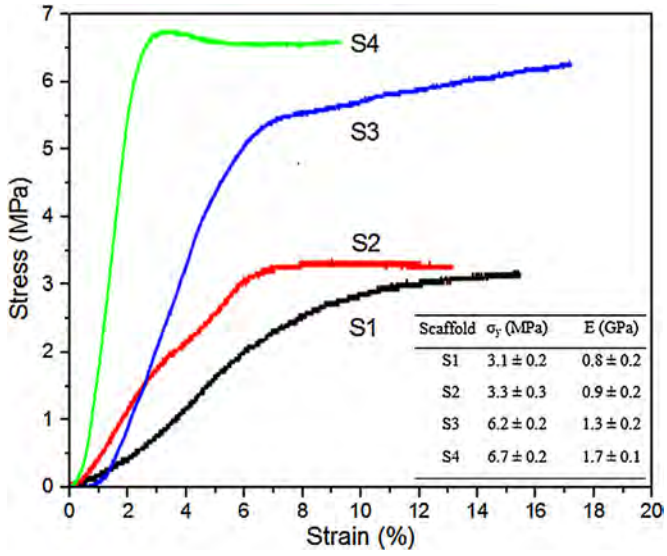

Fig. 4. The stress–strain curves of the prepared nanocomposite scaffolds (S1-S4) in dry state using load and displacement data. Inset shows the mechanical properties consisting of the compressive strength and elastic modulus of the prepared nanocomposite scaffolds, which were measured from stress-strain curves. The elastic modulus is the slope of the initial linear portion, and the compressive strength is the maximum point of the curve.

bonding of TiO_2 overlapped with the mentioned peaks of n-HAp [29]. In addition, the peaks between 900 cm^{-1} and 1100 cm^{-1} displayed an overlap with the two very sharp peaks at 1159 cm^{-1} and 1082 cm^{-1}, which are related to the alcoholic and etheric stretching vibrations of the O—C—O bridge of CS. The characteristic N—H stretching peak of CS appeared at 1658 cm^{-1} has a minor shift due to the graft polymerization [30]. The modifications that took place during the graft polymerization of poly(AAc) onto CS can be confirmed by the presence of a peak at 1562 cm^{-1} related to a C=O groups of poly(AAc) [31]. Also, the peak corresponding to the C—N stretching at 1406 cm^{-1} can support the grafting of AAc onto CS. The sp^3 C—H stretching vibration of the CS backbone and CS-graft-poly(AAc) is observed at 2924 cm^{-1}. The broad absorption peaks between 3000 cm^{-1} and 3700 cm^{-1} are assigned to the stretching vibration of the O—H groups of CS, n-HAp, poly(AAc) and to the probable presence of water. This peak has overlapped with the $-NH_2$ stretching vibration peak of CS. These supportive results confirmed the synthesis of TiO_2 doped in CS-graft-poly(AAc)/n-HAp nanocomposite scaffolds.

3.1.2. X-ray diffraction (XRD) analysis

The XRD diffractograms of the prepared nanocomposite scaffolds were shown in Fig. 2. The XRD patterns of all the prepared samples were almost similar and exhibited the characteristics peaks of CS at around 2θ of 10° and 20°, albeit with low intensity [32]. This reduction in the crystallinity of CS in the nanocomposite scaffolds can be due to the formation of hydrogen bonds and ionic interactions during the graft polymerization of poly(AAc) to CS and the imprinting of n-HAp accompanied by TiO_2 in the network of grafted polymer, which can lead to more disordering in the crystalline region of chitosan [33,34]. In addition, the pattern of all the prepared scaffolds shows the diffraction peaks indicated TiO_2 at 12°, 26°, 38° and 54° in the structure of the prepared scaffolds. However, 2θ angle of TiO_2 deviated from normal TiO_2 X-ray diffraction spectra, due to the molecular rearrangement in structure of nanocomposite [35]. Moreover, the intensity of the peaks corresponded to the CS and TiO_2 decreased with increasing n-HAp content from S1 to S4 sample. This reduction implies that the impact of CS-g-poly(AAc)/TiO_2 in the crystallinity of the prepared

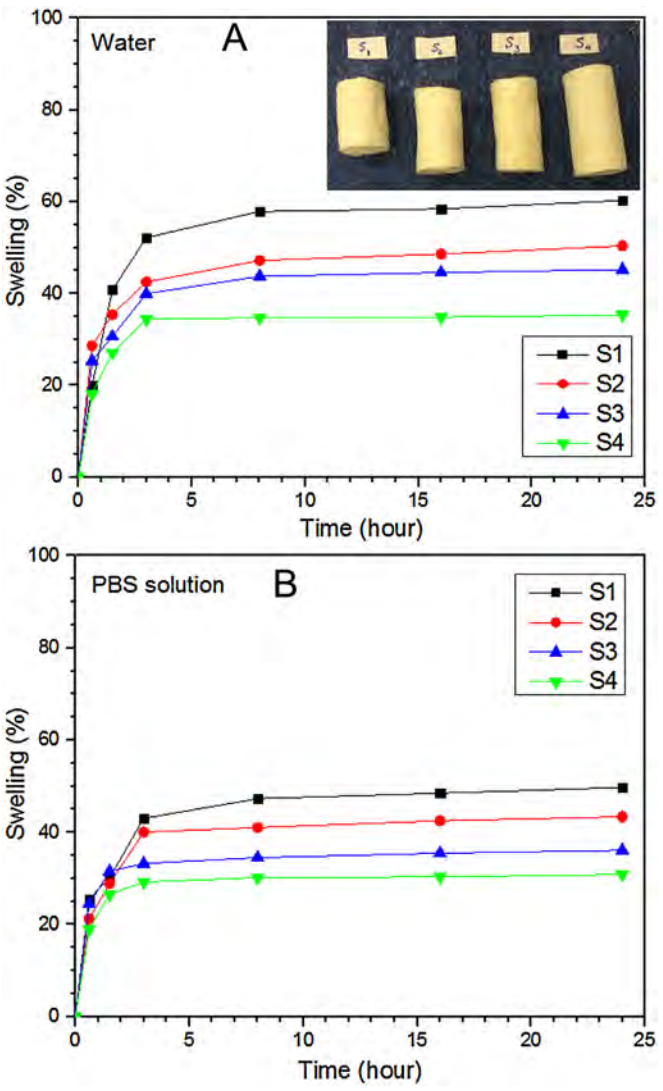

Fig. 5. The swelling behavior of the prepared nanocomposite scaffolds in distilled water and PBS solution were shown [In these experiments, 0.5 g of the prepared nanocomposite scaffolds were immersed in 100 mL of solutions (i.e., water and PBS solution) at 21 °C for 24 h].

nanocomposite scaffolds against n-HAp is too low. According to the previous studies, the X-ray pattern of n-HAp displays crystalline peaks at 2θ of 23.2°, 26°, 29.3°, 32.2°, 46.6°, and 49.4° [36]. It is worth mentioning that an increase in peak height and a decrease in peak width in the XRD patterns of the scaffolds from S1 to S4 confirm the presence of n-HAp with different contents in the structure of the prepared nanocomposite scaffolds.

3.1.3. Scanning electron microscopy (SEM)

The SEM images of the prepared nanocomposite scaffolds in Fig. 3 shows interconnected irregular and random pores with interconnected pores with 44–75 μm diameter range. This microstructure gives an opportunity for possible application of the prepared nanocomposite scaffolds in tissue engineering due to easy seeding cells, entrance of nutrients, oxygen diffusion, blood vessels, growth factors and the exiting of waste [25,33]. Ideal pore sizes depending different cells and tissues. They have various dimensions and an ideal pore sizes should be at least a few times bigger than the cell size [37]. The porosity and average pore size of the prepared nanocomposite scaffolds are listed in Table 1. The pore distribution increased from 55% to 81%, while pore size decreased around 56%

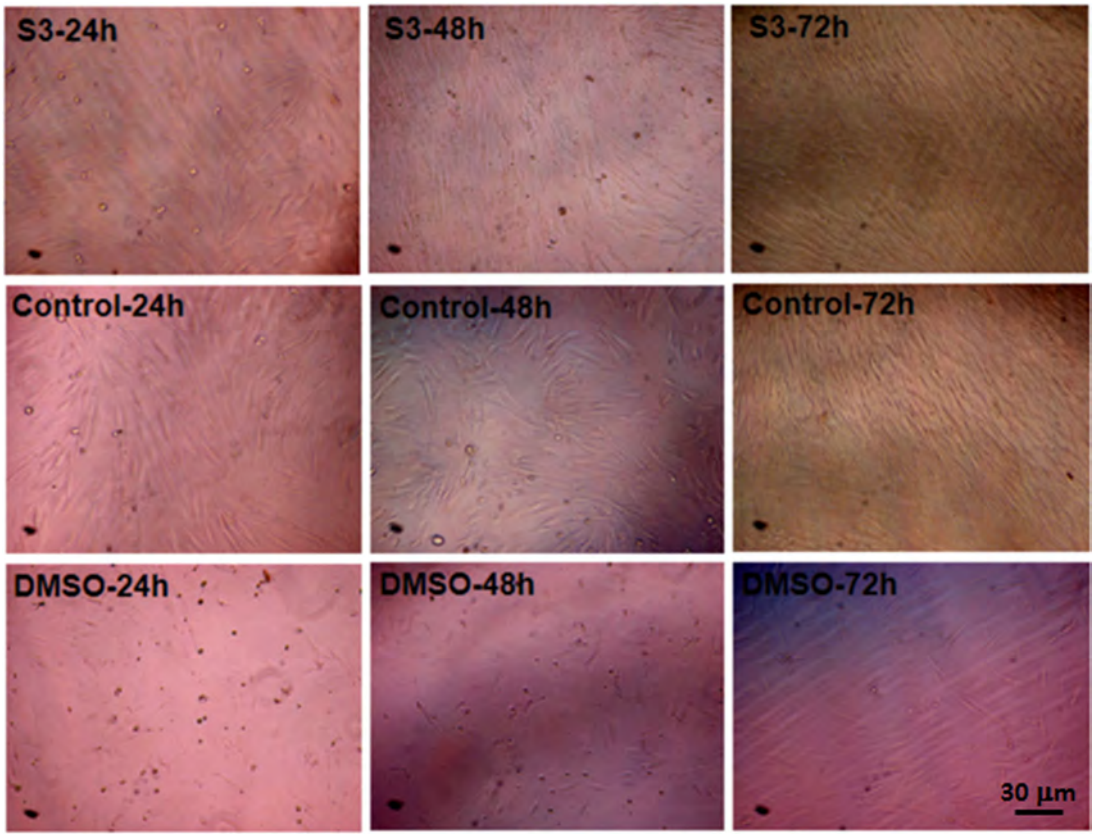

Fig. 6. Optical images of the HuGu cell morphology using an optical microscope in the presence of the S3 scaffold extract ranging from 0.125 to 2.00 mg mL^{-1} after 24, 48, and 72 h were shown. The culture medium was consisted of high-glucose 89% DMEM supplemented with 2 mmol L^{-1} glutamine, 10% FBS, and 1% penicillin. Extracts of the samples were prepared by incubation of the S3 scaffold (0.250–4.00 mg) in culture medium at 37 °C for 24 h. Then, sample extracts with five different concentrations of (0.125–2.00 mg mL^{-1}) were filtered through a 0.2 Lm membrane.

from S1 to S4. This can be justified with an increase in the numbers of HAp nanoparticles in the structure of the prepared nanocomposite scaffolds, which acts as a barrier to prevent exhausting of fluid during freeze drying process and cause an incline in the pore size. In addition, the morphology of the nanocomposite scaffolds revealed that the n-HAp and TiO_2 particles are agglomerated into large clusters and fixed in the CS-graft-poly(AAc) matrix.

By selecting the random place in the SEM images of the S3 sample, the EDS spectrum shows the several signals for carbon, oxygen, nitrogen, calcium, phosphorus, and titanium atoms related to the components of nanocomposite scaffold (i.e., CS, poly(AAc), n-HAp and TiO_2). These results can suggest that the components homogeneously distributed within the pores wall of the scaffolds.

3.2. Mechanical properties of the prepared nanocomposite scaffold

The mechanical properties consisting of the compressive strength and elastic modulus of the prepared nanocomposite scaffolds were measured from stress-strain curves (see Fig. 4). As can be seen, the elastic modulus of scaffolds was increased by increasing the amount of n-HAp in samples S1 to S4 from 0.8 ± 0.2 GPa to 1.7 ± 0.1 GPa. This can be attributed to the higher elastic modulus of n-HAp (i.e., 18 ± 5 GPa) which is approximately 67 wt% of the natural mineral constituent of human bone compared with CS and poly(AAc) (i.e., 30 ± 10 KPa, and 17.9 ± 0.1 MPa, respectively) [38–41]. Therefore, it is expected that sample S4 with the highest amounts of n-HAp has the highest elastic modulus. Also, the highest values of compressive strength (6.7 ± 0.2 MPa) were related to the S4 sample with the highest amount of ceramic phase compared with S1 with 3.1 ± 0.2 MPa. Accordingly, it can be concluded that the mechanical properties of the prepared nanocomposite scaffolds are particularly satisfactory and the obtained mechanical values are in agreement with the range reported for trabecular bone (i.e., compressive strength of 2–6 MPa and elastic modulus of 0.1–0.3 GPa) [42].

3.3. Swelling properties of the prepared nanocomposite scaffold

The wettability and the structural stability of scaffolds play an important role in tissue engineering for cell nutrition and growth. Fig. 5 shows the swelling behavior of the prepared nanocomposite scaffolds in both distilled-water and PBS solution. Among the prepared nanocomposite scaffolds S1 sample with the lowest amount of n-HAp has the maximum swelling percentage and S4 sample with the highest amount of n-HAp has the minimum swelling percentage in both distilled water and PBS solution. Therefore, it can be found out that wettability is inversely proportional to the n-HAp concentration in the network of the prepared nanocomposite scaffold. These results may be due to the relatively low hydrophilicity of n-HAp particles in comparison to CS-graft-poly(AAc) and also the role of n-HAp as a crosslinker [43]. The increased amount of n-HAp resulted in the generation of more crosslink points in the polymeric network, which can lead to a decrease in the elasticity of the nanocomposite and consequently, a decrease in the swelling percentage [44]. As can be seen from the behavior of the prepared nanocomposite scaffolds, at the beginning the water molecules were in contact with the pores of the scaffold and they penetrated inside the scaffold structure and thus the rate of water uptake for all the samples sharply increased. However, the osmotic pressure dif-

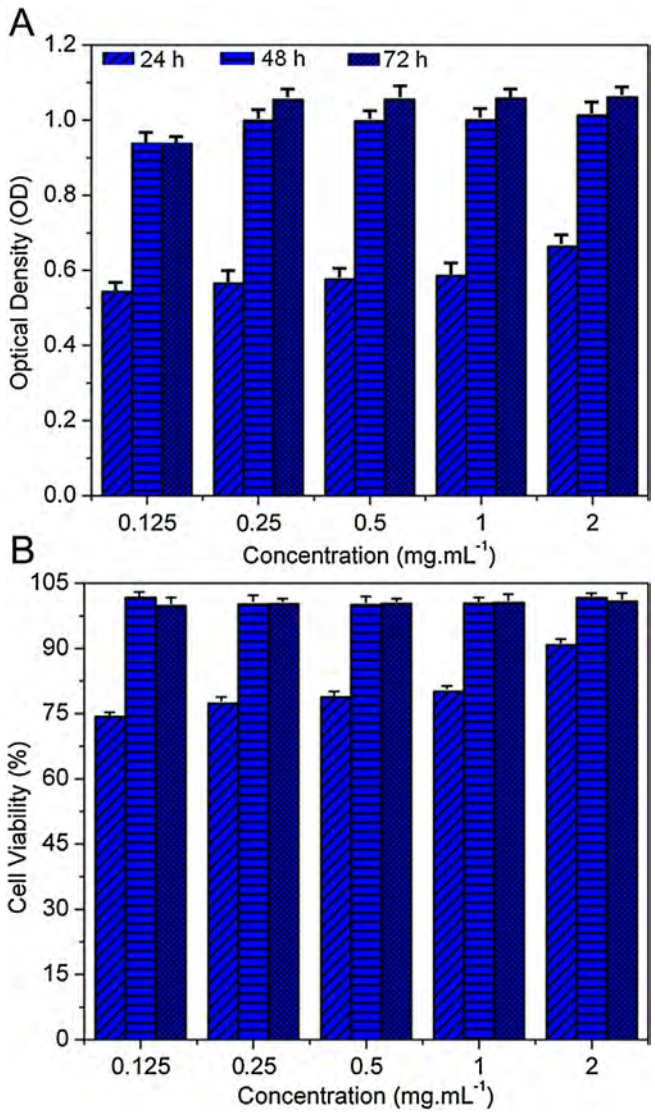

Fig. 7. the result of MTT assay for the S3 scaffold extracts with concentrations ranging from 0.125 to 2.00 mg mL^{-1} in the presence of HuGu cells after 24, 48, and 72 h incubation time at 37 °C, in terms of optical density values (OD) which were recorded at 570 nm by the absorbance microplate reader and the cell viability (%) which were calculated using the Eq. (3).

ference between the solution and the scaffold might be reduced by the increasing water-scaffold interactions, and after passing ~5 h the rate of swelling decreased. Finally, the osmotic force at the equilibrium state was balanced and the big differences in liquid uptake were not observed with further increases in time until it reached a plateau.

3.4. Biocompatibility of the prepared nanocomposite scaffold

It is necessary to consider the cytotoxicity of either the original prepared scaffold or the material that may leach out from them through in vitro assays for biological applications. The cytotoxicity of the prepared scaffold extracts (S3) with 5 different concentrations (from 0.125 mg L^{-1} to 2.00 mg L^{-1}) was estimated by evaluating the viability of HuGu cells using an MTT assay. According to Fig. 6 that shows the optical imaging of the HuGu fibroblastic cells during 72 h of culturing time, the number of cells in the presence of scaffold extracts increased compared to the control (cells without the addition of the scaffolds' extract). After 72 h, the cells were densely arranged and seemed to be pile up on each other. In addition, the results of OD and cell viability in Fig. 7 revealed that the prepared nanocomposite scaffold in each concentration of extract is not cytotoxic. The good cell viability higher than that of control samples indicates a higher proliferation rate.

4. Conclusion

In summary, we report fabrication of novel biocompatible nanocomposite scaffolds for bone tissue engineering applications. The present study investigated the preparation of new nanocomposite scaffolds based on TiO_2 doped in grafted CS/n-HAp using freeze-drying technique. Nano-sized HAp particles had a significant effect on the scaffold structure and proved to be a highly important parameter affecting the mechanical properties of the nanocomposites. Based on our experimental data, the nanocomposite scaffolds showed excellent bioactivity and biocompatibility. Results revealed scaffolds with large pore sizes and high porosities. The S3 nanocomposite scaffold with ideal porosity (i.e., $78 \pm 1\%$) and pore size ($153 \pm 2\ \mu m$) was chosen in favor of cell growth and proliferation. Pure n-HAp scaffold is brittle, but deformability could be gained due to the presence of the CS and poly(AAc). The results obtained from compressive mechanical measurements indicated that the nanocomposite scaffolds have a compressive strength of ~6.5 MPa, similar to the value of the strength of cancellous bone. The results indicated that the prepared nanocomposites in this study are suitable for further development and could be valuable for the fabrication of bone-substitution materials with adjustable mechanical properties.

References

[1] J. Venkatesan, P.A. Vinodhini, P.N. Sudha, S. Kim, Advances in Food and Nutrition Research, Elsevier, 2014.
[2] A.R. Amini, C.T. Laurencin, S.P. Nukavarapu, Crit. Rev. Biomed. Eng. 40 (2012) 363–408.
[3] L. Polo-Corrales, M. Latorre-Esteves, J.E. Ramirez-Vick, J. Nanosci. Nanotechnol. 14 (2014) 15–56.
[4] E. Beniash, Wiley Interdiscip. Rev. Nanomed. Nanobiotechnol. 3 (2011) 47–69.
[5] H.W. Kim, J.C. Knowles, H.E. Kim, J. Biomed. Mater. Res. B 70 (2004) 240–249.
[6] E. Karamian, M.R. Kalantar Motamedi, A. Khandan, P. Soltani, S. Maghsoudi, Prog. Nat. Sci. 24 (2014) 150–156.
[7] S. Saber-Samandari, K.A. Gross, Acta Biomater. 5 (2009) 2206–2212.
[8] S. Saber-Samandari, S. Saber-Samandari, F. Ghonjizade-Samani, J. Aghazadeh, A. Sadeghi, Ceram. Int. 42 (2016) 11055–11062.
[9] S. Saber-Samandari, S. Saber-Samandari, S. Kiyazar, J. Aghazadeh, A. Sadeghi, Int. J. Biolog. Macromol. 86 (2016) 434–442.
[10] H. Wang, Y. Li, Y. Zuo, J. Li, S. Ma, L. Cheng, Biomaterials 28 (2007) 3338–3348.
[11] B.M. Chesnutt, A.M. Viano, Y. Yuan, Y. Yang, T. Guda, M.R. Appleford, J. Biomed. Mater. Res. A 88 (2009) 491–502.
[12] S.N. Danilchenko, O.V. Kalinkevich, M.V. Pogorelov, A.N. Kalinkevich, A.M. Sklyar, T.G. Kalinichenko, J. Biomed. Mater. Res. A 96 (2011) 639–647.
[13] M. Dash, F. Chiellini, R.M. Ottenbrite, E. Chiellini, Prog. Polym. Sci. 36 (2011) 981–1014.
[14] H. Deng, P. Lin, S. Xin, R. Huang, W. Li, Y. Du, Carbohydr. Polym. 89 (2012) 307–313.
[15] I. Olivas-Armendáriz, P. García-Casillas, R. Martínez-Sánchez, A. Martínez-Villafañe, C.A. Martínez-Pérez, J. Alloys Compd. 495 (2010) 592–595.
[16] Y. Wan, X. Cao, S. Zhang, S. Wang, Q. Wu, Acta Biomater. 4 (2008) 876–886.
[17] Y. Wan, J. Gao, J. Zhang, W. Peng, G. Qiu, Polym. Degrad. Stab. 95 (2010) 1994–2002.
[18] R. Sabetrasekh, H. Tiainen, S.P. Lyngstadaas, J. Reseland, H.J. Haugen, J. Biomater. Appl. 25 (2011) 559–580.
[19] H. Tiainen, D. Wiedmer, H.J. Haugen, J. Eur. Ceram. Soc. 33 (2013) 15–24.
[20] E. Karamian, M. Abdellahi, A. Khandan, S. Abdellah, J. Alloys Compd. 679 (2016) 375–383.
[21] H.G. Haugen, M. Monjo, M. Rubert, A. Verket, S.P. Lyngstadaas, J.E. Ellingsen, H.J. Rønold, J.C. Wohlfahrt, Acta Biomater. 9 (2013) 5390–5399.
[22] G.C. Smith, L. Chamberlain, L. Faxius, G.W. Johnston, S. Jin, L.M. Bjursten, Acta Biomater. 7 (2011) 3209–3215.
[23] D.F. Williams, Biomaterials 29 (2008) 2941–2953.
[24] J. Kim, D. Kim, O. Lee, H. Jua, B.M. Lee, H.C. Park, Int. J. Biolog. Macromol. 82 (2016) 160–167.
[25] Q.L. Loh, C. Choong, Tissue Eng. Part B 19 (2013) 485–502.
[26] P. Thevenot, A. Nair, J. Dey, J. Yang, L. Tang, Tissue Eng. Part C 14 (2008) 319–325.
[27] R. Zhang, P.X. Ma, J. Biomed. Mater. Res. 44 (1999) 446–455.

[28] S. Saber-Samandari, K. Alamara, S. Saber-Samandari, K.A. Gross, Acta Biomater. 9 (2013) 9538–9546.
[29] C. Kailasanathan, N. Selvakumar, V. Naidu, Ceram. Int. 38 (2012) 571–579.
[30] S. Saber-Samandari, M. Gazi, O. Yilmaz, Water Air Soil Pollut. 224 (2013) 1624–1631.
[31] Y.T. Xie, A.Q. Wang, Iran. Polym. J. 19 (2010) 131–141.
[32] A. Zare, S. Saber-Samandari, S. Saber-Samandari, Ceram. Int. 42 (2016) 17781–17791.
[33] C.T. Laurencin, L.S. Nair, CRC Press (2014).
[34] S. Saber-Samandari, O. Yilmaz, E. Yilmaz, J. Macromol. Sci. A 49 (2012) 591–598.
[35] K. Thamaphat, P. Limsuwan, B. Ngotawornchai, Kasetsart J. (Nat. Sci.) 42 (2008) 357–361.
[36] S. Saber-Samandari, N. Nezafati, S. Saber-Samandari, Crit. Rev. Ther. Drug Carrier Syst. 33 (2016) 41–75.
[37] G. Wei, P.X. Ma, Biomaterials 25 (2004) 4749–4754.
[38] T. Boudou, O. Jacques, P. Catherine, T. Philippe, Biorheology 43 (2006) 721–728.
[39] S. Jana, S.J. Florczyk, M. Leung, M. Zhang, J. Mater. Chem. 22 (2012) 6291–6299.
[40] S. Saber-Samandari, K. Alamara, S. Saber-Samandari, Ceram. Int. 40 (2014) 563–572.
[41] S. Saber-Samandari, C.C. Berndt, K.A. Gross, Acta Biomater. 7 (2011) 874–881.
[42] S. Lee, M. Porter, S. Wasko, G. Lau, P.Y. Chen, E.E. Novitskaya, A.P. Tomsia, A. Almutairi, M.A. Meyers, J. McKittrick, Mater. Res. Soc. Synp. Proc. 1418 (2012) 177–188.
[43] M. Peter, N. Ganesh, N. Selvamurugan, S.V. Nair, T. Furuike, H. Tamura, R. Jayakumar, Carbohydr. Polym. 80 (2010) 687–694.
[44] V. Asadian, S. Saber-Samandari, S. Saber-Samandari, J. Biomed Mater. Res. A 104 (2016) 2992–3003.